

# Some Metal Oxide-Natural Rubber Composites for Gamma- and Low-Energy X-Ray Radiation Shielding

A. Fisli<sup>1\*</sup>, E. Yulianti<sup>2</sup>, B. Hanurajie<sup>3</sup>, S. G. Sukaryo<sup>1</sup>, Mashadi<sup>2</sup>,  
A. K. Rivai<sup>1</sup>, H. Prastanto<sup>4</sup>, M. I. Fathurrohman<sup>4</sup>

<sup>1</sup>Research Center for Radiation Detection and Nuclear Analysis Technology, National Research and Innovation Agency, KST B. J. Habibie, Serpong 15310, Indonesia

<sup>2</sup>Research Center for Advanced Material, National Research and Innovation Agency, KST B. J. Habibie, Serpong 15310, Indonesia

<sup>3</sup>Directorate of Laboratory Management, Research Facilities, Science and Technology Park, National Research and Innovation Agency, KST B. J. Habibie, Serpong 15310, Indonesia

<sup>4</sup>Research Center for Rubber Technology, Indonesia Rubber Research Institut, Jl. Salah No. 1, Bogor 16151, Indonesia

## ARTICLE INFO

### Article history:

Received 4 January 2022

Received in revised form 17 January 2023

Accepted 17 January 2023

### Keywords:

Polymers composites  
Oxide metal  
Shielding material  
X-ray radiation  
Gamma-ray radiation

## ABSTRACT

This work studied protective material consisting of several metal oxide composites ( $Pb_3O_4$ ,  $WO_3$ ,  $SnO_2$ , and  $Bi_2O_3$ )-natural rubber (NR) for X-ray and gamma-ray shielding. The composites were prepared through open milling and vulcanization processes and further characterized by scanning electron microscope (SEM), X-ray diffraction (XRD), rheometry analysis, and density gauge. The attenuation coefficient of the sample was investigated using X-ray generators with voltages ranging from 50 to 140 kV and gamma-ray energies ranging and 356 to 1250 keV, respectively. The experimental results show that the linear attenuation coefficient of NR filled with metal oxides was significantly improved compared to pure NR. For gamma-ray 661 keV, the HVL of NR decreased from 9.0 cm to between 4.4 - 6.2 cm after it was filled with metal oxides. The  $Bi_2O_3$ -NR is the best suitable material for gamma-ray attenuation, followed by  $Pb_3O_4$ -NR,  $WO_3$ -NR, and  $SnO_2$ -NR. Meanwhile, for x-rays, the HVL of NR decreased from 2.0 cm to between 0.17 -0.31 cm after it was filled with metal oxides. The proposed metal oxide-NR composites can be appropriate as a flexible protective material for manufacturing wearable radiation shielding products such as gloves, aprons, rubber underwear, and other wearable materials.

© 2023 Atom Indonesia. All rights reserved

## INTRODUCTION

Over the past decades, a considerable number of studies have been reported regarding protective materials or radiation shielding for radiation protection purposes, such as pure metals and their alloys [1], concrete [2], glasses [3], and polymeric composites [4]. Polymer-composite-based radiation shielding is a material that commonly consists of heavy metal incorporated into the polymer to enhance its radiation attenuation performance and physical properties [5]. Numerous researchers have developed various polymer-heavy metal composites, including epoxy-Pb, -Bi, or -W [6], PVA- $WO_3$

composites [7], polyimide- $Bi_2O_3$  composite [8], recycled-HDPE-PbO [9], PVC- $Bi_2O_3$  composites [10], polyester- $Bi_2O_3$  [11], geopolymers/slag-fly ash [12], and cassava starch-Pb nitrate [13]. The shielding material based on polymer composite does not enhance the attenuation characteristics compared to introducing pure filler. However, these materials not only attenuate radiation but also possess good physical and chemical properties, including flexibility, lower toxicity, ease of shaping, low weight, better physical durability, and chemical resistance [4,5]. Therefore, these materials possibly provide the benefit of broader and more flexible applications in various environmental settings.

Natural rubber (NR) or latex with the chemical formula  $(C_5H_8)_n$  is an isoprene polymer made of a runny, milky white liquid from a rubber

\*Corresponding author.

E-mail address: [adel.fisli@brin.go.id](mailto:adel.fisli@brin.go.id)

DOI: <https://doi.org/10.55981/aij.2023.1213>

tree (*Hevea brasiliensis*). NR has good elasticity, high flexibility, and high strength compared to other polymer types [14]. In a previous study, NR demonstrated its ability to attenuate radiation sufficiently more highly than other polymers [15]. Numerous works have been carried out to demonstrate flexible radiation shielding materials using metal oxide as filler and NR as the matrix, namely  $\text{Sb}_2\text{O}_3$  [16],  $\text{BaSO}_4$  [17], Pb and Pb/W [18], bismuth oxide ( $\text{Bi}_2\text{O}_3$ ) [19],  $\text{Gd}_2\text{O}_2\text{S}$  [20] and magnetite ( $\text{Fe}_3\text{O}_4$ ) [21]. Indonesia, the world's second-largest NR producer after Thailand, contributes 27 % of global production [22]. Therefore, it is necessary to make maximum efforts to empower the potential of this abundant local natural resource.

This research aims to develop the flexible radiation shielding materials as safe protective jackets for the radiation worker which focused on comprehensively understanding the effects of several metal oxides ( $\text{Pb}_3\text{O}_4$ ,  $\text{WO}_3$ ,  $\text{Bi}_2\text{O}_3$ , and  $\text{SnO}_2$ ) added into the NR. The morphology, X-ray diffraction, rheometric analysis, and density of the composites were investigated. Each composite's attenuation coefficient and half-value length (HVL) were evaluated to gain information on the radiation shielding performance for low energy X-rays and gamma-rays.

## METHODOLOGY

### Materials

The materials used in the experiment were: SIR-20 NR from the Research Center for Rubber Technology; tungsten oxide ( $\text{WO}_3$ ), bismuth (III) oxide ( $\text{Bi}_2\text{O}_3$ ), tin (IV) oxide ( $\text{SnO}_2$ ), and lead (II)(III) oxide ( $\text{Pb}_3\text{O}_4$ ) from Xingu Chem; and: compounding ingredients (zinc oxide ( $\text{ZnO}$ ), stearic acid, trimethyl quinoline (TMQ), mercaptobenzothiazole (MTB) and sulfur). All materials were commercial-grade quality without any further treatment.

### Preparation of NR composites

The preparation of composites consists of two consecutive steps. The first step is mixing the metal oxide (either  $\text{WO}_3$ ,  $\text{Bi}_2\text{O}_3$ ,  $\text{SnO}_2$ , or  $\text{Pb}_3\text{O}_4$ ) and other ingredients into NR under milling using an open two-roll mill Bersotorf, Oving Rotterdam with the speed of slow roll (24 rpm) and friction ratio (1.4) maintained at  $65 \pm 5$  °C. The chemical composition used for each sample is shown in Table 1. The second step is the process of hot compression molding at 150 °C with a hydraulic pressure of 170

kg/cm<sup>2</sup>. In this step, the NR involves vulcanization in molding. Finally, the molded sample was obtained in a sheet form of 150 mm × 150 mm × 2 mm size.

**Table 1.** The composition of the chemical compound used in the experiment (parts per hundred rubber, phr).

No	Chemical compound	phr	Function
1.	NR	100	Matrix
2.	ZnO	6	Activator
3.	Stearic acid	0.5	Activator
4.	Trimethyl Quanoline (TMQ)	2	Activator
5.	Mercaptobenzothiazole (MTB)	0.5	Accelerator
6.	Sulfur	3.5	Cross linker
7.	Metal oxides (either $\text{WO}_3$ , $\text{Bi}_2\text{O}_3$ , $\text{SnO}_2$ , or $\text{Pb}_3\text{O}_4$ )	100	Protection filler

## Characterization

Before the vulcanization process, the composites carried out the rheological measurements using an MDR 2000 moving die rheometer for 20 minutes at 150 °C according to ISO 6502. All NR composites' density and curing characteristics were determined using a density gauge according to ASTM D 297-15 and a moving die rheometer according to ISO 6502-3, respectively. The morphology and the distribution of filler in the composite were investigated using a JEOL 6510 LA scanning electron microscope at 20 kV. The XRD patterns of the filler were recorded with an Empyrean Panalytical diffractometer with  $\text{CuK}\alpha$  radiation and a wavelength of  $\lambda = 1.154$  Å and operated at 40 kV and 30 mA for the  $2\theta$  range of  $10^\circ$ - $80^\circ$  with a scan step of  $0.02^\circ$ .

## Gamma-rays and X-rays attenuation test

The gamma-ray attenuation property of the shielding materials was measured with a gamma spectrometer apparatus using a Canberra HPGe semiconductor detector. Three energy levels of gamma radiation were used for the attenuation test of the shielding, namely 356 keV, 661 keV, and 1250 keV, which are emitted from the standard radionuclide sources of Ba-133, Cs-134, and Co-60, respectively. The 1250 keV value is the average value of the 1173 keV and 1332 keV energies of Co-60 gamma rays. After passing the sample, gamma rays were counted once by a high-purity germanium detector (Canberra) with a 1.8 keV resolution for the 1332 keV gamma ray of Co-60 and a 25 % relative efficiency. The data acquisition time was taken at < 1 % count error. Meanwhile, the X-rays attenuation of the

shielding materials was tested using YXLON SMART EVO 300D portable X-ray generator with the maximum energies of 50 keV, 100 keV, and 140 keV. The images were analyzed using the HD-CR 35 NDT computed radiography (CR) portable imaging plate type scanner with the DtGaect-X software package installed. The diagram with a short description of the whole experiment setting was showed in Fig. 1.

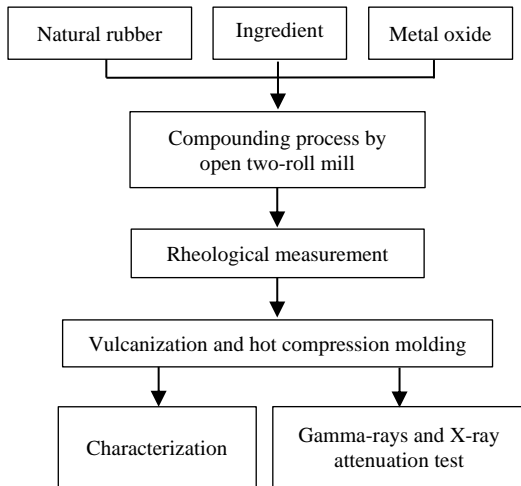


Fig. 1. Diagram with a short description of the experiment setting.

### The theoretical aspect of data analysis

The Beer-Lambert law illustrates the attenuation of a parallel beam of mono-energetic photons by shielding material, as given in Eq. (1) [23].

$$I = I_0 e^{-\mu x} \quad (1)$$

In (1),  $I_0$  is the incident intensity of the photon,  $I$  is the emerging intensity of the photon,  $\mu$  is the linear attenuation coefficient, and  $x$  is the thickness of the shielding material. Further, a straight-line curve was obtained from a relationship of the thickness ( $x$ ) as the abscissa and  $\ln(I/I_0)$  as the ordinate, as described in Eq. (2).

$$\ln \frac{I}{I_0} = -\mu x \quad (2)$$

The shielding performance can also be expressed as the material's HVL, defined as the required thickness of the shielding material to attenuate the photon intensity to 50 % of the incident intensity. It can be written as in Eq. (3).

$$HVL = \frac{\ln 2}{\mu} \quad (3)$$

## RESULTS AND DISCUSSION

Vulcanization is a process of heating rubber in the presence of sulfur to improve the rubber's elasticity and strength. Vulcanized rubber results in three-dimensional cross-linking of the chain rubber molecules (polyisoprene) bonded by sulfur atoms [24,25]. Figure 2 shows the relationship between torque and vulcanization time on metal oxide-NR composites at a temperature of 150 °C. In the initial process, the torque value decreases with increasing temperature due to the changes in the viscosity of the compound. Then, the vulcanization temperature increases with an increase in torque value. It indicates that the rate of the vulcanization reaction increases. This stage is the curing reaction period that the cross-linking network grows in rubber [26]. Metal oxide added to NR increases the maximum torque of the composite.  $\text{Bi}_2\text{O}_3$ -NR composite has the highest maximum torque, followed by  $\text{Pb}_3\text{O}_4$ -NR,  $\text{WO}_3$ -NR, and  $\text{SnO}_2$ -NR composites. This result implies that the presence of metal oxide in the NR increases the chemical cross-linking of the NR. Lim-Aroon et al. reported that metal oxides could act as a co-activator in NR's vulcanization process, which assist in increasing the crosslink density and improving the physical properties (tensile strength and elongation at break) of NR [19].

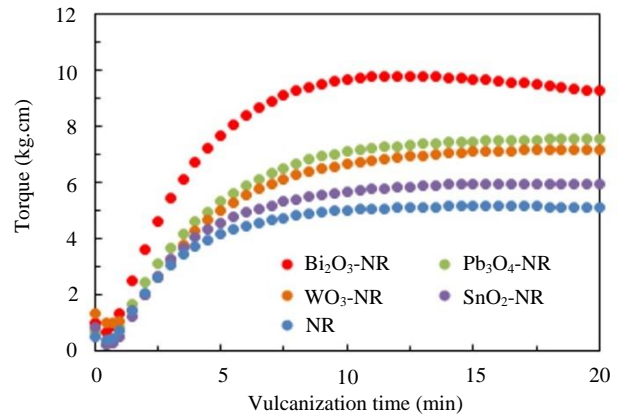
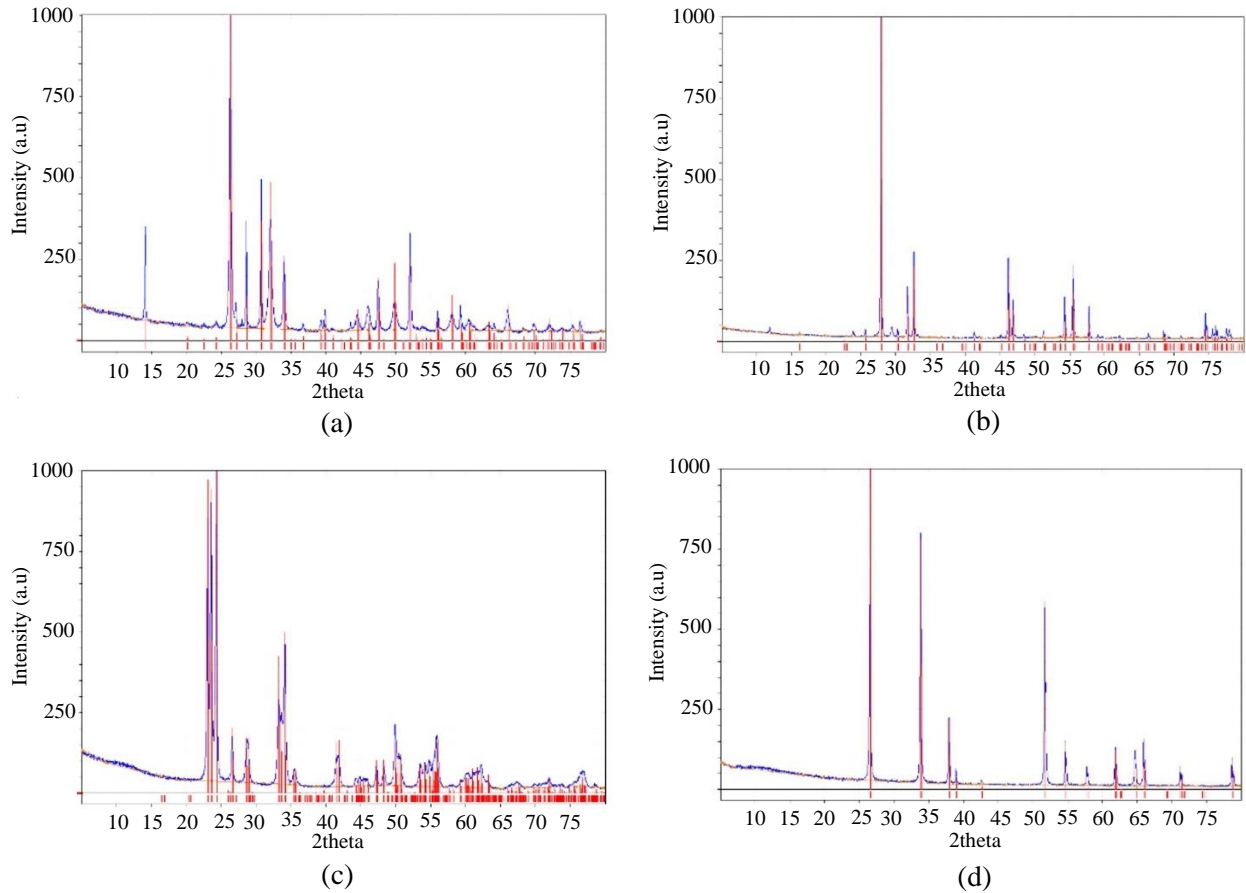


Fig. 2. Torques of the prepared samples as function of vulcanization time at the constant temperature of 150 °C.

The XRD pattern in this study was used for structural analysis and estimation of crystallite size of metal oxides filler. All the peaks of the XRD spectrum were analyzed and indexed using Match Version 3.0. Figure 3 and Table 2 show the phase analysis and crystallite size determination of each metal oxide used. The crystallite size was determined using the Scherrer formula, which calculated it from the full width at half maximum (FWHM) of the strongest reflection peak of each sample. The phase analysis of metal oxides was  $\text{SnO}_2$ ,  $\text{WO}_3$ ,  $\text{Pb}_3\text{O}_4$ , and  $\text{Bi}_2\text{O}_3$  with crystallite sizes of 131 nm, 72 nm, 50 nm, and 299 nm, respectively.

**Table 2.** The phase analysis and crystalline size of various metal oxides used.

No	Symbol element	atom number	phase	molar mass (g.mol <sup>-1</sup> )	density g.cm <sup>-3</sup>	crystal system	crystalline size (nm)	Card number
1.	Sn	50	SnO <sub>2</sub>	150.7	6.95	tetragonal	131	[96-100-0063]
2.	W	74	WO <sub>3</sub>	231.8	7.16	monoclinic	72	[96-210-6383]
3.	Pb	82	Pb <sub>3</sub> O <sub>4</sub>	685.6	8.30	tetragonal	50	[96-153-7984]
4.	Bi	83	Bi <sub>2</sub> O <sub>3</sub>	466.0	8.90	tetragonal	299	[96-901-2328]

**Fig. 3.** XRD diffraction patterns of various metal oxides, (a) Pb<sub>3</sub>O<sub>4</sub>, (b) Bi<sub>2</sub>O<sub>3</sub>, (c) WO<sub>3</sub>, and (d) SnO<sub>2</sub>.

SEM technique is used to observe the morphology and the distribution of metal oxide in the natural rubber matrix. The typical SEM image of various metal oxides and their composites is shown in Fig. 4. It can be seen that Pb<sub>3</sub>O<sub>4</sub> particles were larger (around 1000 nm) and with a more irregular-agglomerate shape than others (Fig. 4(a)). Bi<sub>2</sub>O<sub>3</sub> particles possessed a spherical shape with uniform distribution of around 300 nm in size (Fig. 4(b)). Meanwhile, the WO<sub>3</sub> and the SnO<sub>2</sub> particles have a spherical agglomeration shape with the smaller distribution of around 200 nm in size (Figs. 4(c) and (d)). Preferably, metal oxides used have the same particle size and shape but are very difficult to obtain.

Figure 5 shows the SEM images of metal oxides embedded into the NR matrix. The contrast of brightness was observed in SEM photos. It indicates the difference in the atomic numbers of the composite constituents. The metal oxide fillers have high atomic number, and they appear in brighter grayscale tone. In

contrast, the NR matrix, whose constituent elements have low atomic numbers, shows a slightly darker gray. This figure depicts that the filler (seen as white patches) is surrounded by and evenly distributed in the NR matrix. Thus, the filler has been successfully distributed in the NR matrix for all variable samples. It can be interpreted as indicating good interfacial adhesions between the NR and the metal oxide phase.

The high density of radiation shielding material gives significant interaction probability for X-rays and gamma rays, resulting in better shielding performance. Figure 6 shows the density of prepared composites. The density of NR was 0.978 g/cm<sup>3</sup>. When it was implanted with filler material, the density of the composite increased to the range of 1.625 g/cm<sup>3</sup> to 1.690 g/cm<sup>3</sup>. The density of the composites increased by around 70 % compared to NR due to the high density of the filler implanted in the NR (Table 2). Bi<sub>2</sub>O<sub>3</sub>-NR has the highest density, followed by Pb<sub>3</sub>O<sub>4</sub>-NR, WO<sub>3</sub>-NR, and SnO<sub>2</sub>-NR.

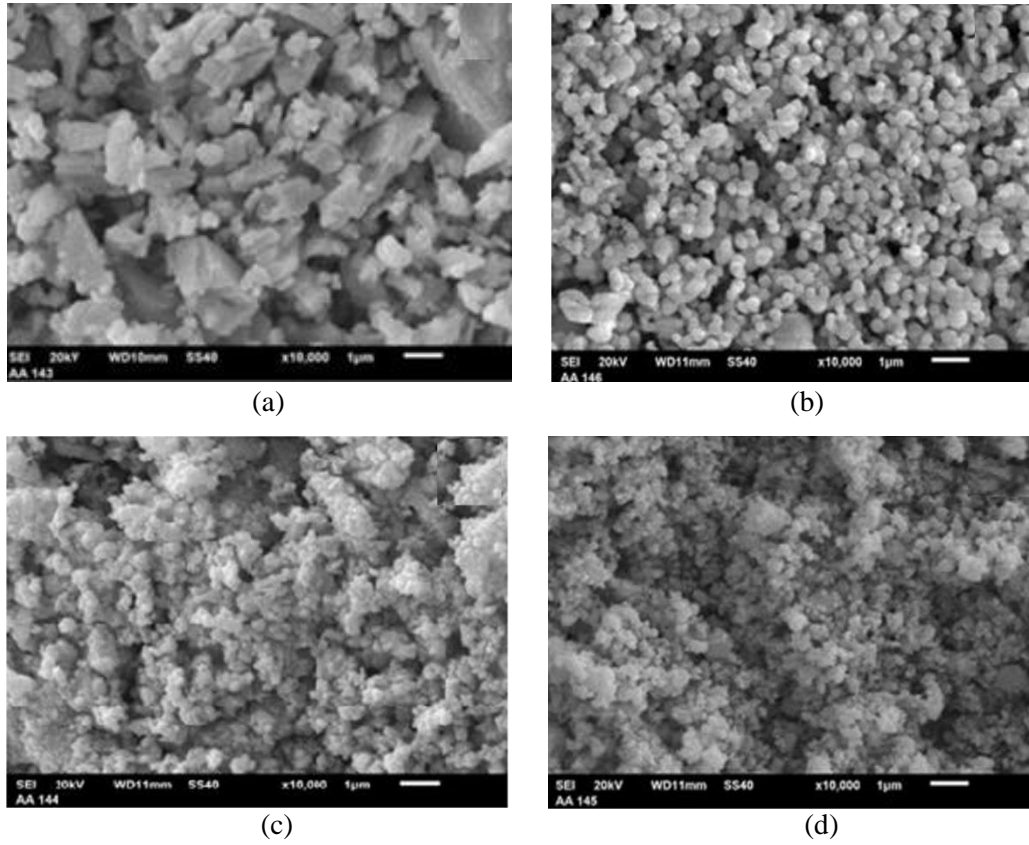


**Fig. 4.** The typical SEM image of various metal oxides; (a)  $Pb_3O_4$ , (b)  $Bi_2O_3$ , (c)  $WO_3$ , and (d)  $SnO_2$ .

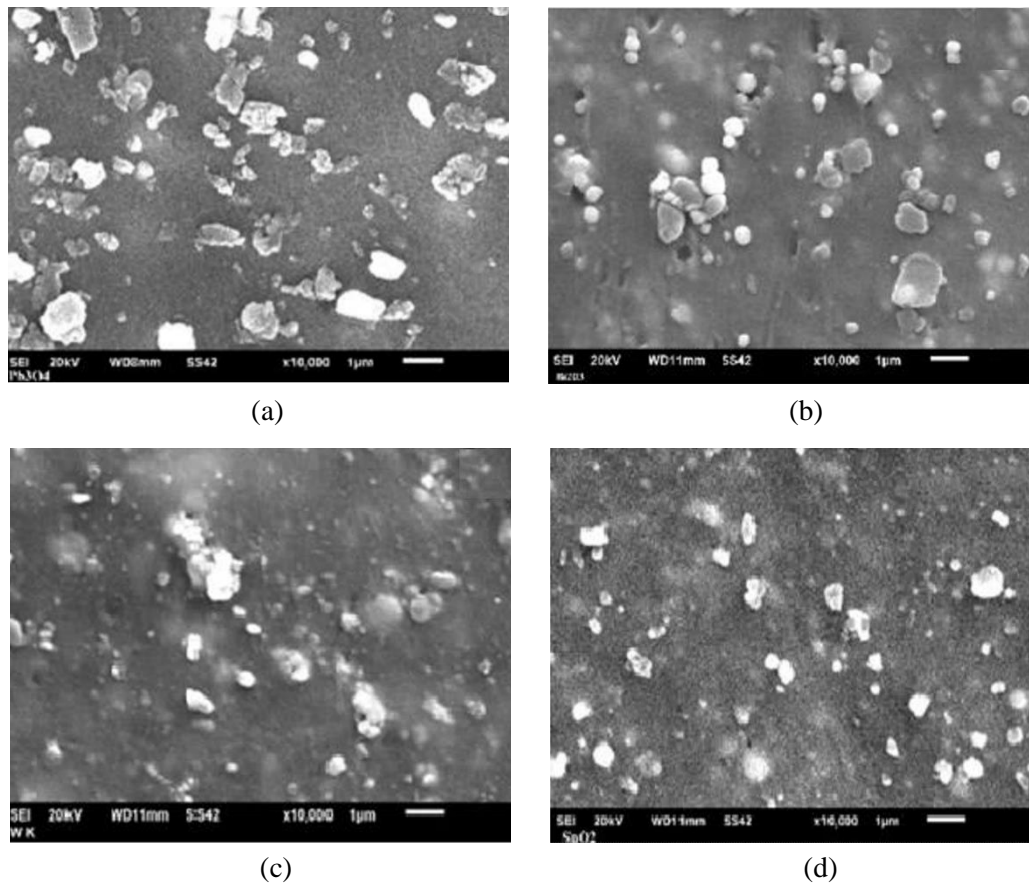


**Fig. 5.** The typical SEM image of composites; (a)  $Pb_3O_4$ -NR, (b)  $Bi_2O_3$ -NR, (c)  $WO_3$ -NR, and (d)  $SnO_2$ -NR.

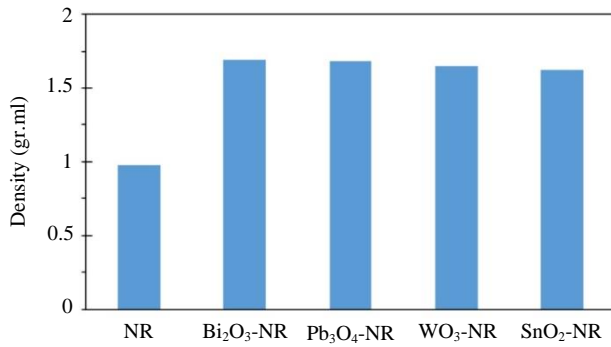


Fig. 6. The density of prepared composites.

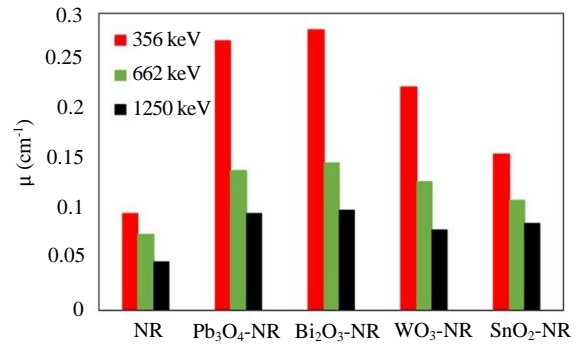


Fig. 8. The  $\mu$  value of the NR composites for 359 keV, 661 keV, and 1250 keV gamma rays.

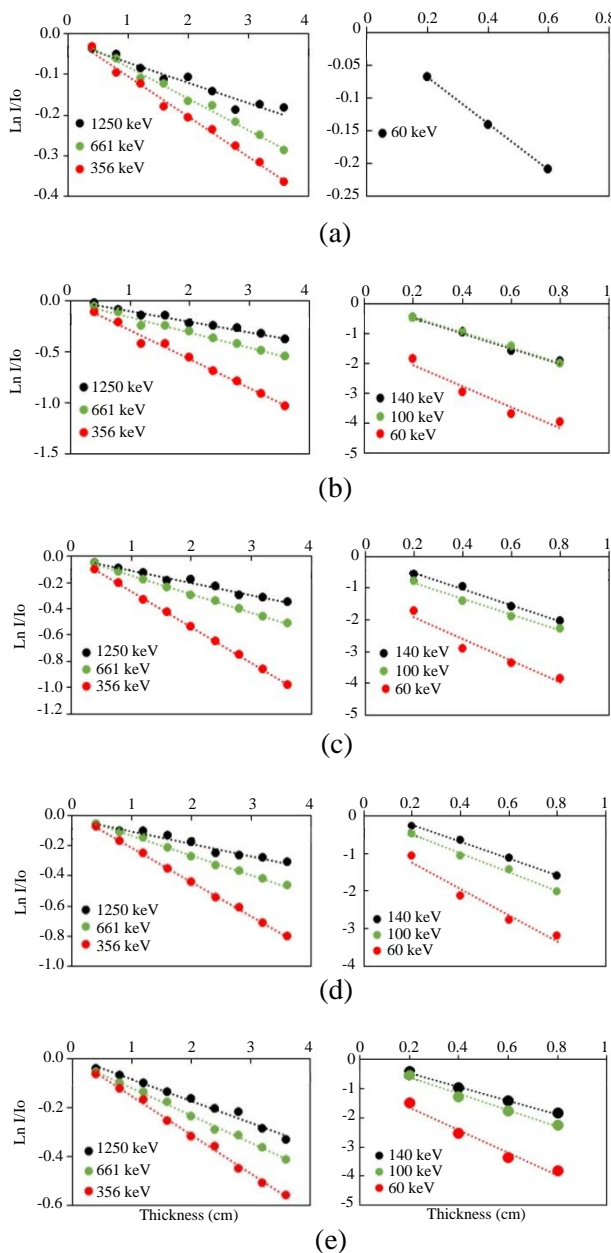


Fig. 7. The plots of  $\ln(I/I_0)$  vs. shielding thickness for the prepared sample at various gamma ray energies and X-ray peak energies; (a) NR, (b)  $Pb_3O_4$ -NR, (c)  $Bi_2O_3$ , (d)  $WO_3$ -NR, and (e)  $SnO_2$ -NR.

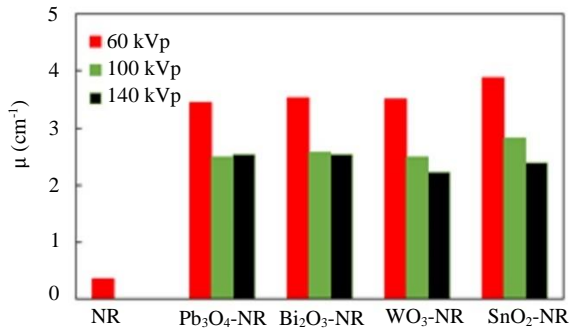


Fig. 9. The  $\mu$  values of the NR composites for low-energy X-rays.

The linear relation between  $\ln(I/I_0)$  and sample thickness  $x$  is shown in Fig. 7. The regression lines exhibit good statistical fits with  $R^2$  values above 0.99. The  $\ln(I/I_0)$  value decrease with the increase of the shielding thickness. The thicker the shielding materials, the longer the radiation path in the composites, the higher the collision probability, and the more the photon intensity is attenuated.

The linear attenuation coefficient  $\mu$  is determined from the slope of the linear relation between  $\ln(I/I_0)$  and sample thickness  $x$ . It can be expressed as the product of the number of atoms in a one cubic centimeter of the shielding material and the probability of photons being scattered or absorbed by the nucleus or electrons of an atom of the shielding material. The larger the  $\mu$  value is, the better the shielding performance of materials is. Figure 8 shows the  $\mu$  value for gamma radiation for various NR composites. The experiment indicated that  $\mu$  increased after the NR was filled with metal oxides. The magnitude of  $\mu$  depends on the metal oxide types used in the following order;  $Bi_2O_3$ -NR >  $Pb_3O_4$ -NR >  $WO_3$ -NR >  $SnO_2$ -NR > NR. These results are in line with the literature that  $\mu$  increases with atomic number ( $Z$ ) of the element used as filler and with the density of the material [27].

For the low energy X-rays, the presence of metal oxides in NR significantly affects the attenuation coefficient, as shown in Fig. 9. The  $\mu$  value of NR composites increases drastically, up to 10 times that of the pure NR. In the low-energy region, the photoelectric

interaction is more dominant than Compton scattering and pair production; therefore, the photon is more attenuated. The  $\mu$  values are slightly different among metal oxides used. It is difficult to determine the main factor in attenuating X-rays. Besides the atomic number and density, other factors such as the particle size and the dispersion uniformity of the filler in the polymer matrix probably play a significant role in attenuating low energy photons [28]. El-Khatib et al. [29] reported that nano-CdO particles in HDPE would ultimately lead to a better performance of the gamma radiation shielding compared to micro-CdO particles. The homogeneous dispersion of the metal oxides in the matrix is obtained in the presence of good compatibility between the metal oxides and the polymer matrix, resulting in synergistic effect in the composite [30]. In addition, the porosity formed during the manufacturing process with different types and particle size filler significantly differed for each shielding material. It can also affect the shielding performance [31].

The attenuation effectiveness of the NR composite sample can be expressed in terms of the HVL, as shown in Fig. 10. The lower the HVL is, the more effective the shielding material is. The pure NR has HVL values of 7.1 cm, 9.0 cm, and 14.1 cm for gamma-ray energy of 356 keV, 661 keV, and 1250 keV, respectively. This HVL value is higher than that reported El-Khatib et al. [18] with the result of 6.2 cm and 7.6 cm for gamma-ray energy of 356 keV and 661 keV. That is because El-Khatib uses an NR type with a higher density (1.073 g/cm). After NR was filled with metals oxides, their HVL decreased to the range of 2.4 cm to 4.4 cm, 4.6 cm to 6.2 cm, and 6.9 cm to 8.5 cm for gamma-ray energies of 356 keV, 661 keV, and 1250 keV, respectively. The magnitude of HVL depends on the oxide used. The lowest HVL was found for Bi<sub>2</sub>O<sub>4</sub>/NR, followed by Pb<sub>3</sub>O<sub>4</sub>/NR, WO<sub>3</sub>/NR, and SnO<sub>2</sub>/NR. This result similar to those reported by Onjun et al. [32] and Intom et al. [33], that lead oxide filled NR at the same composition exhibit HVL value of 4.5 and 4.4 cm, respectively, for gamma-ray energy of 661 keV.

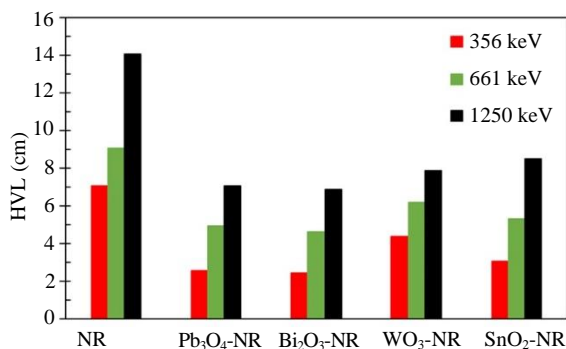


Fig. 10. The calculation results of HVL for gamma rays for several NR composites.

The attenuation test results for the X-rays are shown in Fig. 11. The HVL value drastically decreased after NR was filled by metal oxide. The HVL of NR was 2.0 cm for maximum X-ray energy of 60 keV. After the NR was filled by metal oxide, the HVL value decreased to 0.17 cm to 0.20 cm, 0.24 cm to 0.28 cm, and 0.27 cm to 0.31 cm for maximum X-ray energies of 60 keV, 100 keV, and 140 keV, respectively. Thus, the shielding thickness can be saved by around 85 % to 90.5 % for those X-ray energies after NR is filled by metal oxides.

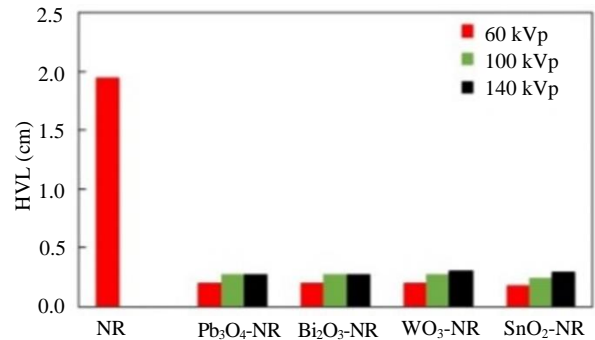


Fig. 11. The calculation results of HVL for low energy X-rays for several NR composites.

## CONCLUSION

The flexible radiation shielding materials of metal oxide-NR composites have been successfully fabricated as protective materials for low-energy X-ray and gamma-ray radiation. The density of NR increases after it is filled with metal oxide. As an equivalent of pure NR, introducing some metal oxide as absorbing fillers reduced the shielding thickness by approximately 84 % to 91 % for low energy X-rays and 38 % to 66 % for the energy gamma-ray. The Bi<sub>2</sub>O<sub>3</sub>-NR composite exhibits the best performance for gamma rays, followed by Pb<sub>3</sub>O<sub>4</sub>-NR, WO<sub>3</sub>-NR, and SnO<sub>2</sub>-NR. Meanwhile, for X-ray, SnO<sub>2</sub>-NR has the lowest HVL value, followed by Bi<sub>2</sub>O<sub>3</sub>-NR, Pb<sub>3</sub>O<sub>4</sub>-NR, and WO<sub>3</sub>-NR. These composites could be used as various flexible products of shielding materials such as gloves, aprons, rubber underwear, and other wearable materials.

## ACKNOWLEDGMENT

This research was supported by research and development of radiation shielding programs of DIPA Grants at Research Center for Radiation Detection and Nuclear Analysis Technology, Research Organization for Nuclear Energy - National Research and Innovation Agency, as the implementation of collaborative research activities between the Research Centre for Radiation Detection and Nuclear Analysis and Indonesia Rubber Research Institute.

## AUTHOR CONTRIBUTION

The first author (Adel Fisli) contributed as the main contributor of this paper, responsible for conducting the paper, data collection, data analysis, and experiment. The other author contributed to preparing the sample, characterization, the attenuation test of gamma-rays and X-rays, and data analysis. All authors contributed to reading and approving the final version of the paper.

## REFERENCES

1. T. Kaur, J. Sharma and T. Singh, Prog. Nucl. Energy **113** (2019) 95.
2. M. A. Khalaf, C. C. Ban and M. Ramli, Constr. Build. Mater. **215** (2019) 73.
3. P. Kaur, D. Singh and T. Singh, Nucl. Eng. Des. **307** (2016) 364.
4. S. Nambiar and J. T. W. Yeow, ACS Appl. Mater. Interfaces **4** (2012) 5717.
5. C. V. More, Z. Alsayed, M. S. Badawi et al., Environ. Chem. Lett. **19** (2021) 2057.
6. N. Z. N. Azman, S. A. Siddiqui and I. M. Low, Appl. Phys. A Mater. Sci. Process. **110** (2013) 137.
7. M. A. Hosseini, S. Malekie and F. Kazemi, *Investigating of Shielding Characteristics of Polyvinyl Alcohol/Tungsten Oxide Composite (PVA / WO<sub>3</sub>) for Gamma Rays of 133Ba*, First National Conference on Micro/nanoscale Technologies (2018) 1.
8. V. I. Pavlenko, N. I. Cherkashina and R. N. Yastrebinsky, Heliyon **5** (2019) e01703.
9. M. E. Mahmoud, A. M. El-Khatib, M. S. Badawi et al., J. Cleaner Prod. **176** (2018) 276.
10. A. G. Nuñez-Briones, R. Benavides, E. Mendoza-Mendoza et al., Radiat. Phys. Chem. **179** (2021) 109198.
11. M. R. Ambika and N. Nagaiah, Indian J. Adv. Chem. Sci. **2** (2017) 23.
12. M. W. Hassan, S. Sugiharto and S. Astutiningsih, Atom Indones. **47** (2021) 173.
13. E. Afrianti, D. Tahir, B. Y. E. B Jumpeno et al., Atom Indones. **47** (2021) 129.
14. K. Sriroth, S. Liengprayoon and S.T Semegen, *Natural Rubber (Hevea): Elastomeric Properties*, in: Reference Module in Materials Science and Materials Engineering, Elsevier (2017) 1.
15. R. R. Bhosale, C. V. More, D. K. Gaikwad et al., Nucl. Technol. Radiat. Prot. **32** (2017) 288.
16. S. Yonphan, W. Chaiphaksa, E. Kalkornsuraprane et al., Radiat. Phys. Chem. **200** (2022) 110379.
17. N. N. Plangpleng, P. Charoenphun, D. Polpanich et al., Radiat. Phys. Chem. **199** (2022) 110311.
18. A. M. El-Khatib, A. S. Doma, M. S. Badawi et al., Mater. Res. Express **7** (2020) 105309.
19. P. Lim-Aroon, E. Wimolmala, N. Sombatsompop et al., IOP Conf. Ser. Mater. Sci. Eng. **526** (2019) 012015.
20. M. M. Panitra, F. Aziz, A. K. Rivai et al., AIP Conf. Proc. **2381** (2021) 020054-1.
21. D. Toyen, A. Rittirong, W. Poltabtim et al., Iran. Polym. J. **27** (2018) 33.
22. D. Kopeliovich, Substances & Technologies. [https://www.substech.com/dokuwiki/doku.php?id=vulcanization\\_of\\_rubber.Report\\_Digital.pdf](https://www.substech.com/dokuwiki/doku.php?id=vulcanization_of_rubber.Report_Digital.pdf). Retrieved in January (2022).
23. Y. Wang, G. Wang, T. Hu et al., Nucl. Eng. Technol. **52** (2020) 1565.
24. T. H. Khang and Z. M. Ariff, J. Therm. Anal. Calorim. **109** (2012) 1545.
25. M. I. Fathurrohman, D. R. Maspanger and S. Sutrisno, Bull. Chem. React. Eng. Catal. **10** (2015) 104.
26. E. Seliga, O. Bošák, P. Košťál et al., J. Phys. Conf. Ser. **602** (2015) 012010.
27. S. Kaewjaeng, N. Kothan, H. J. Chanthima et al., Mater. Today Proc. **5** (2018) 14901.
28. M. Saiyad, N. M. Devashrayee and R. K. Mevada, Polym. Compos. **35** (2014) 1263.
29. A. M. El-Khatib, M. I. Abbas, M. A. Elzaher et al., Sci. Rep. **9** (2019) 1.
30. G. G. Kaya and H. Deveci, *4 - Design and synthesis of metal oxide-polymer composites*. Metal Oxides, Renewable Polymers and Polymer-Metal Oxide Composite, S. Haider and A. Haider (Eds.), Elsevier, Netherlands (2022) 101.
31. S. C. Kim and S. H. Cho, Appl. Sci. **9** (2019) 1765.
32. O. Onjun, N. Buasuwan, T. Rungseesumran et al., J. Phys. Conf. Ser. **1285** (2019) 012048.
33. S. Intom, E. Kalkornsuraprane, J. Johns et al., Radiat. Phys. Chem. **172** (2020) 108772.